Available online at www.sciencedirect.com

ScienceDirect

Proceedings of the Combustion Institute 35 (2015) 1417–1424

Proceedings of the Combustion Institute

www.elsevier.com/locate/proci

Fuel effects on leading point curvature statistics of high hydrogen content fuels

Andrew Marshall *, Julia Lundrigan, Prabhakar Venkateswaran, Jerry Seitzman, Tim Lieuwen

Georgia Institute of Technology, Atlanta, GA 30332, USA

Available online 2 August 2014

Abstract

Fuel composition has significant influences on the turbulent flame speed of mixtures with strong stretch sensitivity. These fuels effects are associated with reactant thermal-diffusive properties and stretch sensitivities, causing local variations in the burning rate along the flame front. This study is motivated by leading point descriptions of the turbulent flame speed, which argue that S_T is controlled by the flame characteristics at its positively curved leading edge. It has been argued that the leading edge of the flame approaches "critically stretched" values in thermo-diffusively unstable flames, implying that the appropriate laminar flame speed to parameterize the turbulent flame speed is the maximum flame speed across all potential values of flame stretch, $S_{L,max}$, as opposed to its unstretched value, $S_{L,0}$. This paper describes an experimental investigation of the characteristics of the flame leading point in high stretch sensitivity flames to assess this hypothesis more fully. Measurements of the flame curvature were obtained with a low swirl burner (LSB) for several H_2/CO mixtures at velocities from 30–50 m/s. These data show that the leading point conditioned curvature statistics are a strong function of the turbulence intensity of the flow. Counter to our expectations, however, the measurements show relatively weak influences of fuel composition on the leading point curvature of the turbulent flame front. As such, these results do not seem consistent with prior arguments that the increased turbulent flame speeds seen with increasing hydrogen content are the result of increasing flame curvature/stretch rates, and therefore $S_{L,max}$ values, at the flame leading points. Additional analysis is needed to understand the physical mechanisms through which the turbulent flame speed is altered by differential diffusion effects.
Published by Elsevier Inc. on behalf of The Combustion Institute.

Keywords: Stretch effects; Flame curvature; Leading points; High hydrogen content; Fuel effects

1. Introduction

The objective of this paper is to improve the understanding of turbulent flame propagation characteristics of high stretch sensitivity, premixed flames. Early models of the turbulent flame speed use the form:

* Corresponding author. Address: Ben T. Zinn Combustion Laboratory, 635 Strong Street NW, Atlanta, GA 30318, USA. Fax: +1 404 894 0888.
E-mail address: andrew.marshall@gatech.edu (A. Marshall).

http://dx.doi.org/10.1016/j.proci.2014.07.034
1540-7489/Published by Elsevier Inc. on behalf of The Combustion Institute.

$$S_T = S_{L,0} f(u'/S_{L,0}) \quad (1)$$

where $S_{L,0}$ is the unstretched laminar flame speed and u' is the turbulence intensity [1,2]. However, studies have shown that S_T is also affected by turbulent length scales [3], bulk flow velocity [4], experimental configuration [5,6], and fuel composition [2,7–9]. Of particular interest to this paper is the effect of fuel composition, which has been well-documented in the literature [2]. For example, our group has reported measurements of H_2: CO blends showing factor of three variations in S_T across fuel blends with identical $S_{L,0}$ values, even at turbulence intensities $u'_{rms}/S_{L,0}$ up to 40. Similar observations were made by Karpov et al. [10], Wu et al. [11], Bradley et al. [12], Kido et al. [7,13], Brutscher et al. [14] and others, and summarized in the review of Lipatnikov and Chomiak [2].

The sensitivity of S_T to fuel composition is associated with the stretch sensitivity of the reactant mixture, which leads to variations in the local consumption speed along the turbulent flame front. This stretch sensitivity can arise from non-unity Lewis number and preferential diffusion effects [15]. In Particular, the high mass diffusivity of H_2 makes H_2-bearing mixtures highly stretch sensitive, such as shown in the illustrative calculations in Fig. 1. These calculations, which include detailed kinetics and transport mechanisms, incorporate both non-unity Lewis number and preferential diffusion effects. While various modeling approaches have been put forth for capturing these stretch sensitivities, leading points concepts appear to be a particularly natural approach for describing them. Leading points concepts were proposed by Zel′dovich [16] and expanded upon by a number of groups, as summarized by Lipatnikov and Chomiak [2]. Leading points are the positively curved (convex to the reactants) points on the flame front that propagate out farthest into the reactant mixture and can be shown to control the overall propagation velocity of the turbulent flame under certain conditions [3]. This can be shown, for example, by applying the Kolmogorov–Petrovskii–Piskunov (KPP) theorem [17] to the propagation of a one-dimensional turbulent premixed flame in frozen turbulence, where, under certain circumstances, S_T is controlled by the conditions at the leading edge of the flame brush, defined as the point where $\langle c \rangle \rightarrow 0$ [18,19].

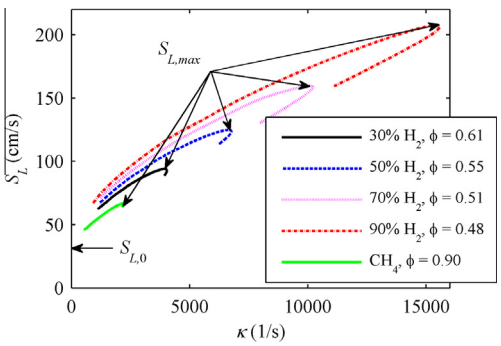

Fig. 1. Opposed flow geometry stretch sensitivity calculations of H_2:CO fuel blends and CH_4 [20].

Leading points ideas are particularly revealing for negative Markstein length mixtures, as calculations of laminar flame stretch sensitivities show that the positively curved leading point flame speed can substantially exceed $S_{L,0}$, as shown in Fig. 1 [15]. Assuming S_T is controlled by the leading point characteristics, the ensemble averaged laminar burning rate of this leading point turns out to be a very significant turbulent flame property. Directly following these ideas, Venkateswaran et al. [9,20] developed a scaling law for the turbulent flame speed of negative Markstein length flames, using the maximum stretched laminar flame speed, $S_{L,max}$, as the normalizing parameter, as opposed to the traditional approach of using the unstretched laminar flame speed, $S_{L,0}$. The form of this scaling law is given by:

$$\frac{S_T}{S_{L,\max}} \leq 1 + \frac{u'_{LP}}{S_{L,\max}} \quad (2)$$

where u'_{LP} is the turbulence intensity at the leading point of the flame. An example $S_{L,max}$ calculation for an opposed flow, strained flame configuration is shown in Fig. 1 The dynamical significance of $S_{L,max}$ in negative Markstein length mixtures arises from the fact that this velocity/strain rate at the leading point is a steady-state 'attractor' for constant density flames with positively curved wrinkles [20]. This idea that $S_{L,max}$, and not $S_{L,0}$, is the suitable velocity scale for correlating S_T was suggested by [3] and has found justification in data from Venkateswaran et al. [20], as shown in Fig. 2, which plots data obtained with a range of H_2:CO mixtures normalized by $S_{L,0}$ (Fig. 2a) and $S_{L,max}$ (Fig. 2b). Note the strong fuel effects manifested in the $S_{L,0}$ scaled data, but the good collapse of the data using the $S_{L,max}$ scaling.

However, questions remain concerning the application of leading points ideas to data. Of particular focus for this paper is the fact that the scaling in Fig. 2 is "global" in nature and work is needed to assess key assumptions of the leading point model concerning local attributes of the flame. For example, Fig. 1 clearly shows the monotonic increase in $S_{L,max}$ with increasing H_2 content. However, it also shows that the flame stretch rate at $S_{L,max}$ varies strongly with H_2 content, a prediction that can be evaluated from computations or measurements. If the physical arguments leading to this scaling approach are correct, then the flame stretch characteristics at its leading points should exhibit systematic differences that scale with S_T. Particularly, Fig. 1

suggests that mixtures with higher S_T values should have leading points with higher stretch rates. The objective of this study is to evaluate this hypothesis, by determining the curvature characteristics of the flame leading point, and determining whether systematic differences exist that correlate with the measured turbulent flame speeds. This is done by obtaining measurements from a high turbulence intensity burner fueled with several H_2/CO blends, and comparing the flame leading edge characteristics across these fuels.

2. Main body

2.1. Methods

The low swirl burner (LSB) is a useful geometry for local measurements of turbulent flame characteristics, and has been recommended as a canonical geometry for turbulent displacement speed measurements [21]. The LSB was developed by Cheng et al. [22] as a method of generating a freely propagating flame that does not rely on flow recirculation for flame stabilization; the flame stabilizes where the flame speed matches the axial velocity. The flame brush in the central region is flat, providing a close approximation to a statistically 1-D planar turbulent flame [23]. The experiments in this work were performed for H_2:CO mixtures over a wide range of conditions outlined in Table 1.

2.1.1. Experimental facility

The LSB nozzle used in this research is shown in Fig. 3a. Turbulence is generated with the variable turbulence generator detailed in Marshall et al. [24]. Thus, the turbulence intensity can be varied on-the-fly, without changing the bulk flow velocity or replacing blockage plates. The swirler, shown in Fig. 3b, is similar to Cheng's [25] except the central channel blockage plate was removed. Air flow rates through each channel are adjusted by independent valves. This adds the benefit of being able to vary the swirl number S on-the-fly. S is defined as the ratio of angular to axial flow momentum nondimensionalized by the burner radius Rb [26] and has a value of approximately 0.58. Mean flow velocities quoted in this paper are defined as $U_0 = \dot{m}/\rho A$, where $\dot{m}$ is the total mass flow rate, ρ is the reactant density, and A is the area of the exit tube.

2.1.2. Optical diagnostics

Velocity characterizations were obtained using particle image velocimetry (PIV). A Litron Lasers Ltd. LDY303He Nd:YLF twin head frequency doubled laser with a wavelength of 527 nm is used. The camera is a Photron FASTCAM SA1.1 high-speed camera with a full resolution of 1024×1024 pixels at repetition rates up to 5 kHz. Velocity calculations were performed using DaVis 7.2 software from LaVision. The interrogation window size used in the calculations was 32×32 pixels with an overlap of 50%, giving a spatial resolution of approximately 2 mm between adjacent vectors. See Marshall et al. [27] for more details on the PIV setup.

2.1.3. Chemical kinetic calculations

This section describes the calculation approaches used for relating S_T values to detailed kinetic properties of the mixture. Estimates of the unstretched laminar flame speed, $S_{L,0}$, and thickness, $\delta_{f,0}$, were determined using the PREMIX module [28] in CHEMKIN with the Davis mechanism [29]. The flame thickness is calculated using:

$$\delta_{f,0} = \frac{T_b - T_u}{(dT/dx)_{max}} \tag{3}$$

where T_b and T_u and the burned and unburned temperatures, respectively. To determine the response of the mixtures to stretch, symmetric, opposed-flow premixed flame simulations were performed using the OPPDIF module with an arc-length continuation approach [30] in CHEMKIN. Typical calculation results are shown in Fig. 1. Note the flame's sensitivity to high stretch is not a unique function of stretch rate, but depends on the stretch profile through the flame. Thus, the geometry of the model, as well as unsteadiness, influences these results, points discussed in greater detail in our other works [9,31].

2.1.4. Flame front topology

Mie scattering from the PIV experiments is used to estimate the instantaneous flame front positions [32]. The resolution is 0.11 mm/pixel, smaller than the critically stretched flame thickness for the pure hydrogen case of $\delta_{f,crit} = 0.16$mm. Note that PIV gives a 2D slice of an inherently 3D flow field and flame surface. By assuming isotropy, 3D mean statistics can be estimated from 2D information, e.g., $\langle 1/R \rangle_{3D} = \pi/2 \langle 1/R \rangle_{2D}$[33]. Indeed, recent experimental work by Kerl et al. [34] have shown that 2D and 3D measured quantities have qualitatively similar PDFs and are correlated to each other. Finally, Gashi et al. [35] compared curvature from 2D OH-PLIF and 3D DNS data and found

Table 1
Experimental parameters and conditions for the datasets acquired using PIV.

Experiments	H_2:CO
Swirl number, S	0.58
Mean flow velocity, U_0 (m/s)	30, 50
Fuel Composition (% H_2)	50, 70, 100
$S_{L,0}$ (cm/s)	34

that the PDF's were qualitatively similar, with the 3D DNS giving similar, but broader, distributions, as expected based on the above expression. Thus, while 2D data cannot be used to obtain absolute measurements of leading edge curvature, it can be used for examining trends associated with changing fuel composition, the focus of this study.

Figure 4 demonstrates the procedure used for analyzing these images. The raw image, shown in Fig. 4a, is median-filtered using a 5×5 filter to obtain Fig. 4b. Once filtered, the image is binarized with the threshold intensity selected using Otsu's method [36], as shown in Fig. 4c, to separate reactants from products and find the flame edge. Figure 4c shows the resulting instantaneous progress variable c field, which is defined to be 0 in the reactants and 1 in the products [37]. The flame edge, shown in green in Fig. 4d, is quantified by the arc length s, which is calculated from the x- and y-coordinates of the flame edge found from binarization of the image. The curvature is given by:

$$\frac{1}{\mathcal{R}} = \frac{y'x'' - x'y''}{\left((x')^2 + (y')^2\right)^{3/2}} \tag{4}$$

where $(\,)'$ denotes derivatives with respect to the arc length s. Flame curvature is positive when the flame is convex to the reactants. This edge is smoothed with spline curves over an arc length interval ds. The choice of interval length ds is important. If the value of ds is too small, the spline curves will capture pixelation and noise artifacts in the image. If the value of ds is too large, the spline curves effectively filter out high curvature values. We used a value of $ds = (\pi/2)\delta_{f,0}$, following Lee et al. [38]. We also performed a sensitivity analysis of the generated statistics to ds and found insignificant changes with a factor of two decrease in ds, indicating that this choice of ds is fully resolving the curvatures. For a given edge, the cubic smoothing spline, $f_p(x)$, is found from minimizing [39]:

$$p\sum_{i=1}^{N} w_j\left(y_i - f_p(x_i)\right)^2 + (1-p)\int_{x_1}^{x_N}\left(f_p''(x)\right)^2 dx \tag{5}$$

where p, the smoothing parameter, is determined using the generalized cross-validation estimate [40]. The resulting parameterized curve is overlaid onto the raw image in red in Fig. 4d.

Two definitions of the leading point are considered. The first definition, the "instantaneous leading points," are defined as the points on the flame front that penetrate the farthest into the reactants, and are extracted by finding the minimum y-value of the edge at each time instance, removing realizations where this location occurs at the edge of the domain. A representative instantaneous leading point is identified by the yellow x in Fig. 4d. The second definition, the "flame brush leading points," are the points where $\langle c\rangle \to 0$, motivated by application of the KPP theorem, as discussed earlier. Of course, in any finite size data set, a vanishing number of experimental realizations occur as the $\langle c\rangle \to 0$ point, so the flame characteristics were estimated by analyzing flame properties conditioned upon $0 < \langle c\rangle < 0.1$ and $0 < \langle c\rangle < 0.01$. The relationship between these two leading point definitions can be understood from Fig. 4d, which overlays average progress variables on top of the instantaneous flame front. In addition, Fig. 5 presents a PDF of the location of the instantaneous leading point in $\langle c\rangle$-space for several fuel compositions; for reference, the average location of the instantaneous leading point occurs at $\langle c\rangle \cong 0.25$.

3. Results and discussion

Table 2 presents the key operational conditions and summarizes measured results presented in this paper, reporting turbulence intensities, $u'_{ax}/S_{L,0}$, turbulent local displacement speeds, $S_{T,LD}/S_{L,0}$, and mean and standard deviations of the curvature at the leading points. Although not shown, integral length scales were calculated from the velocity fields and have values of roughly 3 mm. They were found to remain roughly constant across all conditions. Although these blends have nominally the same $S_{L,0}$ value, note the increase in measured $S_{T,LD}$ with hydrogen content, similar to the turbulent global consumption speed, $S_{T,GC}$, results shown in Fig. 2a.

3.1. Global (unconditioned) curvature statistics

To provide global baselines, Fig. 6 plots curvature PDFs over the entire extracted surface (i.e., $0 \le \langle c\rangle \le 1$) for the three fuel compositions. From this plot, it is evident that overall flame curvature statistics are only weak functions of fuel composition. While there is a slight preference for positive curvatures, the PDFs are nearly symmetric about zero, consistent with other measurements [38,41–46]. The curvature PDFs tend to shift towards more positive curvatures as the amount of H_2 in the fuel increases. However, the minor differences in curvature PDFs make it hard to explain the approximate 50% measured increase in $S_{T,LD}$ from a 50:50 H_2:CO mixture to a pure H_2 mixture shown in Table 2. The top axis of Fig. 6 plots the curvature normalized by the unstretched flame thickness of the pure H_2 mixture.

While the effect of fuel composition on the curvature PDFs is weak, turbulence intensity has a much stronger effect, as shown in Fig. 7. The figure shows the clear broadening of the curvature PDF, indicating increased occurrence of shorter length scale flame wrinkles, consistent

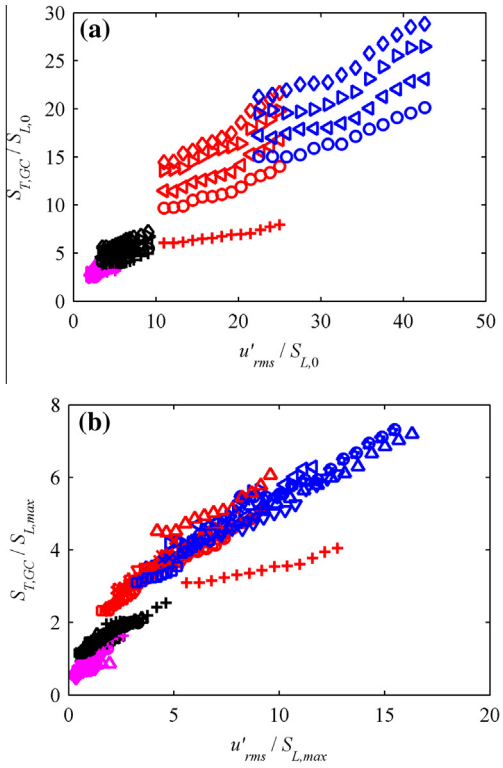

Fig. 2. (a) Measured dependence of the turbulent flame speed, $S_{T,GC}$, upon turbulence intensity, u'_{rms}, normalized by $S_{L,0}$ at various conditions for several H_2:CO ratios and pure CH_4. (b) $S_{T,GC}$ data from (a) normalized by $S_{L,max}$. See Venkateswaran et al. [20] for details on experimental conditions.

with previous studies [38,41–44,47,48]. Similar broadening of the PDFs is also observed for the other fuel compositions studied.

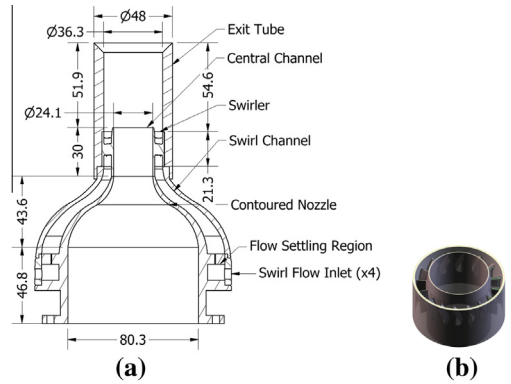

Fig. 3. Detail view of the (a) LSB nozzle and (b) swirler. Dimensions in mm.

3.2. Leading point curvature statistics

This section presents curvature PDFs conditioned on the leading point of the flame and is the key contribution of this study. Figure 8 shows instantaneous leading point characterizations for three fuel compositions. Note that curvatures at instantaneous leading points are positive, as must be the case by geometric necessity. The measured $S_{T,LD}/S_{L,0}$ are, in order of increasing H_2 content, 25.2, 28.5, and 37.5 – thus, $S_{T,LD}$ varies by ~50%. These plots show that the resolved curvature at the instantaneous leading point of the flame is weakly influenced by fuel composition. The mean curvature and its standard deviation increase by only 7% from the lowest to highest H_2 content, as tabulated in Table 2. Similarly, Fig. 9 presents curvature PDFs conditioned on the flame brush leading point for three different fuel compositions over $0 \leq \langle c \rangle \leq 0.01$. These

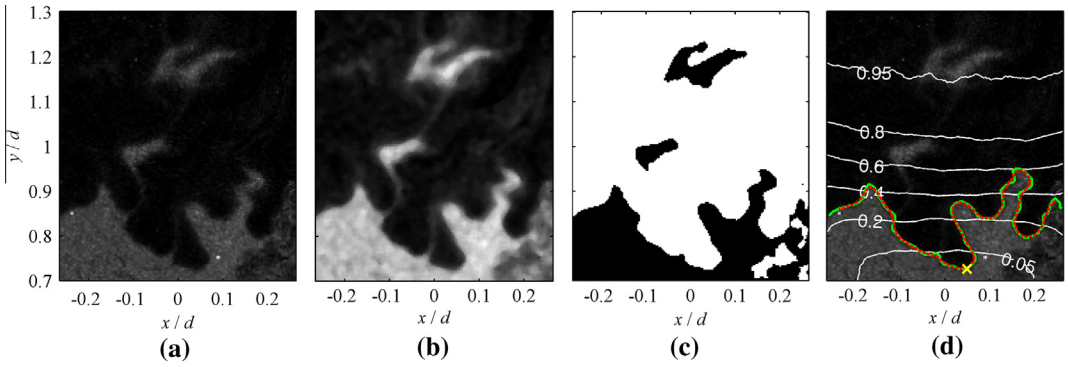

Fig. 4. Post-processing procedure used to identify the flame edge from Mie scattering. (a) raw image, (b) median-filtered image, (c) thresholded image used to identify reactants and products and find the flame edge, and (d) leading flame edge (solid green), fitted spline curve (dashed red), instantaneous leading point (yellow x) and average progress variable, $\langle c \rangle$, (white) overlaid onto raw image (50:50 H_2:CO fuel mixture, $U_0 = 30$ m/s, $\phi = 0.55$). (For interpretation of the references to color in this figure legend, the reader is referred to the web version of this article.)

Table 2
Local displacement turbulent flame speeds, $S_{T,LD}/S_{L,0}$, average curvature, $\overline{1/\mathcal{R}}$, and standard deviation of the curvature, $\sigma_{1/\mathcal{R}}$, at the instantaneous leading points (ILP) and at the flame brush leading points (FBLP). Uncertainties are for a 95% confidence interval.

	$\frac{u'_{ax}}{S_{L,0}}$	$\frac{S_{T,LD}}{S_{L,0}}$	ILP		FBLP ($0 \leq \langle c \rangle \leq 0.1$)		FBLP ($0 \leq \langle c \rangle \leq 0.01$)	
			$\overline{1/\mathcal{R}}$ (mm^{-1})	$\sigma_{1/\mathcal{R}}$ (mm^{-1})	$\overline{1/\mathcal{R}}$ (mm^{-1})	$\sigma_{1/\mathcal{R}}$ (mm^{-1})	$\overline{1/\mathcal{R}}$ (mm^{-1})	$\sigma_{1/\mathcal{R}}$ (mm^{-1})
50% H_2	4.8	9.4	0.88 ± 0.01	0.63	0.32 ± 0.004	0.91	0.40 ± 0.02	0.90
$\varphi = 0.55$	6.6	19.8	1.24 ± 0.02	1.01	0.29 ± 0.005	1.12	0.31 ± 0.02	1.02
$ds = 0.95$ mm	7.2	17.7	1.09 ± 0.02	0.81	0.34 ± 0.005	1.04	0.53 ± 0.02	0.98
	9.4	25.2	1.47 ± 0.03	1.20	0.32 ± 0.006	1.30	0.44 ± 0.03	1.34
70% H_2	3.8	15.4	0.93 ± 0.01	0.64	0.35 ± 0.004	0.88	0.49 ± 0.02	0.74
$\varphi = 0.51$	6.4	23.0	1.25 ± 0.02	0.98	0.29 ± 0.006	1.21	0.76 ± 0.07	1.15
$ds = 0.88$ mm	6.5	19.6	1.13 ± 0.02	0.82	0.33 ± 0.005	1.30	0.52 ± 0.02	0.97
	9.3	28.5	1.51 ± 0.03	1.22	0.29 ± 0.006	1.37	0.39 ± 0.04	1.33
100% H_2	4.9	17.3	0.94 ± 0.02	0.64	0.33 ± 0.004	0.92	0.42 ± 0.02	0.84
$\varphi = 0.46$	6.5	22.9	1.24 ± 0.02	0.93	0.32 ± 0.005	1.15	0.48 ± 0.05	0.95
$ds = 0.83$ mm	6.8	24.9	1.15 ± 0.02	0.79	0.33 ± 0.005	1.13	0.46 ± 0.02	1.07
	11.3	37.5	1.58 ± 0.03	1.28	0.28 ± 0.006	1.42	0.52 ± 0.05	1.33

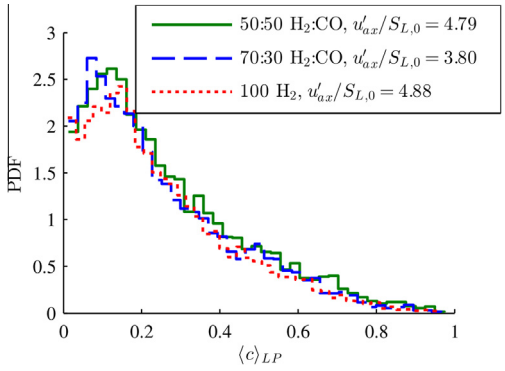

Fig. 5. PDF of locations of instantaneous leading points in ⟨c⟩-space for three different fuel compositions.

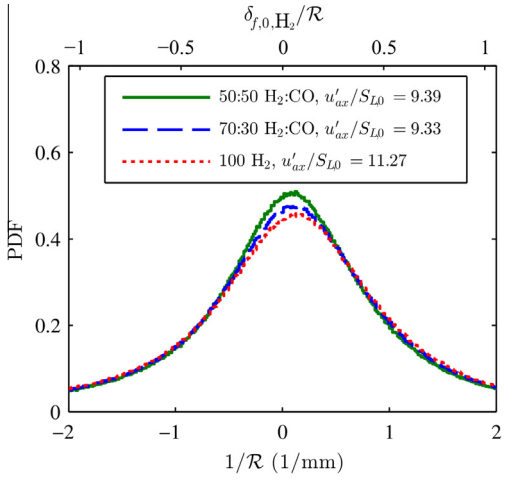

Fig. 6. Unconditioned curvature PDFs ($0 \leqslant \langle c \rangle \leqslant 1$) for varying fuel compositions at $U_0 = 50$ m/s. Secondary top-axis shows curvature normalized by the unstretched flame thickness for the 100% H_2 case.

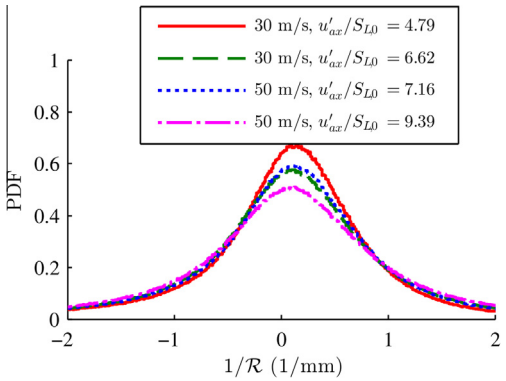

Fig. 7. Unconditioned curvature PDFs ($0 \leqslant \langle c \rangle \leqslant 1$) at varying turbulence intensities for a 50:50 H_2:CO mixture.

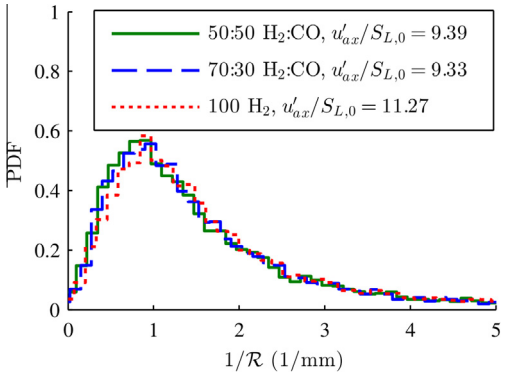

Fig. 8. Instantaneous leading point curvature PDFs for varying fuel compositions at $U_0 = 50$ m/s.

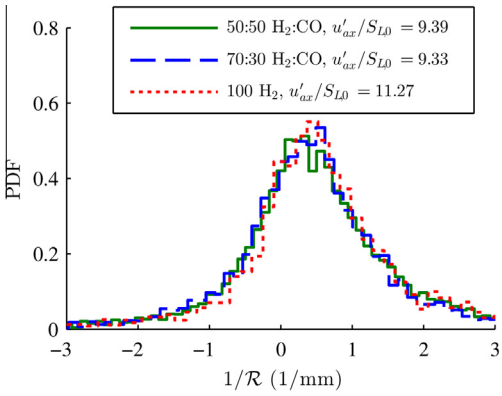

Fig. 9. Flame brush leading point curvature PDFs for varying fuel compositions at $U_0 = 50$ m/s for .

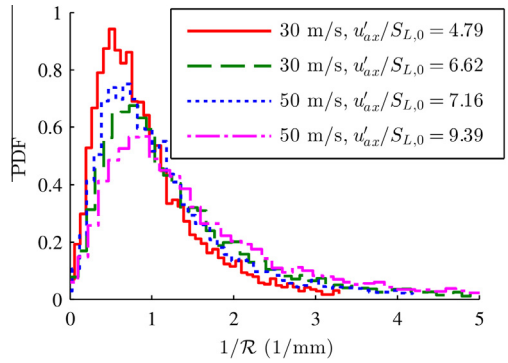

Fig. 10. Instantaneous leading point curvature PDFs at varying turbulence intensities for a 50:50 H_2:CO mixture.

results again show only mild changes in the PDFs with changing fuel composition. Table 2 shows that for the progress variable range $0 \leq \langle c \rangle \leq 0.1$ the mean curvature actually decreases by 13% while the standard deviation of the curvature increases by only 9% with increasing H_2 content. For $0 \leq \langle c \rangle \leq 0.01$ the mean curvature increases by 18% and the standard deviation does not change with increasing H_2 content. The changes observed for both instantaneous and flame brush leading point curvatures are small compared to those calculated for the critically stretched flames in Fig. 1 where, over the same range of fuel compositions, the stretch rate associated with $S_{L,\max}$ varies by 140%.

Of course, even if the curvature at the leading points does not vary with fuel composition, the local consumption speed of the leading points will still increase with the stretch sensitivity of the mixture, which can be observed in Fig. 1 (i.e., the laminar flame speed increases with H_2 content at a fixed stretch rate). Furthermore, the curvature-induced strain rate, κ_c, also increases, even if the average radius of curvature does not change, since $\kappa_c = S_L/\mathcal{R}$. The strain sensitivity calculations in Fig. 1 were used to estimate the magnitude of this effect by estimating the laminar flame speed using $\kappa_c = S_L/\mathcal{R}$. This calculation shows that the time-average strain rate at the instantaneous leading points increases by 39% and the calculated laminar consumption speed increases by approximately 20% from the 50% H_2 mixture to the pure H_2 mixture. Over the same fuel composition range, the strain rate at $S_{L,max}$ increases by 133%, $S_{L,max}$ increases by 65% and $S_{T,LD}$ increases by 50%. Thus, the measured variations are much weaker than the calculated increase of local consumption speed at $S_{L,max}$ or the observed increases in $S_{T,LD}$.

We also include sensitivities of leading point curvature to turbulence intensity. Figure 10 plots the PDFs of instantaneous leading point curvatures at varying turbulence. The results show that as the turbulence increases, the PDF broadens in the direction of short length leading edge flame wrinkles. As tabulated in Table 2, the mean curvature of the 50% H_2 mixture increases from 0.88 to 1.47 1/mm (~67%) over this 96% increase in turbulence intensity. Thus, these results show that statistically significant differences in leading point curvature do occur and are resolved by these measurements.

4. Concluding remarks

The objective of this research was to improve understanding of the turbulent flame leading points in order to test the validity of leading points models for collapsing S_T data. Specifically, we assessed arguments that increasing turbulent flame speeds, observed with high H_2 fuels, were due to higher $S_{L,max}$, and therefore higher flame stretch rates at the leading points. The data presented in this paper show some variation in leading edge stretch rate with fuel composition, but with significantly smaller changes than expected based upon measured increases in S_T and calculated increases in $S_{L,max}$. In contrast, curvature statistics, both global and leading edge-conditioned, exhibit clear sensitivities to turbulence intensity.

Given the strong sensitivities of the turbulent flame speeds of these same mixtures, these data raise the question of how the fuel composition influences the burning rates. Further measurements in other facilities are needed to test the universality of this result. In addition, while these data have focused on curvature, corresponding measurements of the tangential strain rate at the flame leading edge are needed. These results show that further work is needed to understand the physical processes through which S_T is altered by differential diffusion effects.

Acknowledgements

This research was supported by the University Turbine Systems Research (contract #DE-FC21-92MC29061) program and the Air Force Office of Scientific Research (contract #FA9550-12-1-0107/RC657); contract monitors are Dr. Mark Freeman and Dr. Chiping Lee, respectively.

References

[1] A.N. Lipatnikov, J. Chomiak, *Prog. Energ. Combust. Sci.* 28 (2002) 1–74.
[2] A.N. Lipatnikov, J. Chomiak, *Prog. Energ. Combust. Sci.* 31 (2005) 1–73.
[3] V.R. Kuznetsov, V.A. Sabel'nikov, *Turbulent combustion of a homogenous mixture*, in: P.A. Libby (Ed.), *Turbul. and Combust.*, Hemisphere Publishing Corporation, New York, Washington, Philadelphia, London, 1990, pp. 235–251.
[4] S.A. Filatyev, J.F. Driscoll, C.D. Carter, J.M. Donbar, *Combust. Flame.* 141 (2005) 1–21.
[5] J.F. Driscoll, *Prog. Energ. Combust. Sci.* 34 (2008) 91–134.
[6] R.K. Cheng, *Turbulent combustion properties premixed syngas*, in: T.C. Lieuwen, V. Yang, R.A. Yetter (Eds.), *Synth. Gas. Combust: Fundam. Appl.*, CRC Press, 2009, pp. 129–168.
[7] M. Nakahara, H. Kido, *AIAA J.* 46 (2008) 1569–1575.
[8] H. Kido, M. Nakahara, J. Hashimoto, D. Barat, *JSME Int. J. Ser. B Fluids Therm. Eng.* 45 (2002) 355–362.
[9] P. Venkateswaran, A. Marshall, J. Seitzman, T. Lieuwen, *Proc. Combust. Inst.* 34 (2013) 1527–1535.
[10] V.P. Karpov, E.S. Severin, *Combust. Explos. Shock Waves* 16 (1980) 41–46.
[11] M.S. Wu, S. Kwon, J.F. Driscoll, G.M. Faeth, *Combust. Sci. Technol.* 73 (1990) 327–350.
[12] D. Bradley, A.K.C. Lau, M. Lawes, *Philos. Trans. Phys. Sci. Eng.* 338 (1992) 359–387.
[13] H. Kido, M. Nakahara, K. Nakashima, J. Hashimoto, *Proc. Combust. Inst.* 29 (2002) 1855–1861.
[14] T. Brutscher, N. Zarzalis, H. Bockhorn, *Proc. Combust. Inst.* 29 (2002) 1825–1832.
[15] C.K. Law, *Combust. Phys.*, Cambridge University Press, New York, 2006.
[16] Y.B. Zel'dovich, D.A. Frank-Kamenetskii, *Turbulent and heterogeneous combustion*, Moscow Institute of Mechanical Engineering, Moscow, 1947.
[17] A. Kolmogorov, I. Petrovskii, N. Piskunov, *Bjul. Moskovskogo Gos. Univ.* 1 (1937) 1–26.
[18] B. Hakberg, A.D. Gosman, *Symp. (Int) on Combust* 20 (1985) 225–232.
[19] J.M. Duclos, D. Veynante, T. Poinsot, *Combust. Flame.* 95 (1993) 101–117.
[20] P. Venkateswaran, A. Marshall, D.H. Shin, et al., *Combust. Flame.* 158 (2011) 1602–1614.
[21] F. Gouldin, R.K. Cheng, available at <http://energy.lbl.gov/aet/combustion/workshop/workshop.html>.
[22] C.K. Chan, K.S. Lau, W.K. Chin, R.K. Cheng, *Symp. (Int) on Combust* 24 (1992) 511–518.
[23] R.K. Cheng, *Combust. Flame.* 101 (1995) 1–14.
[24] A. Marshall, P. Venkateswaran, D. Noble, J. Seitzman, T. Lieuwen, *Exp Fluids.* 51 (2011) 611–620.
[25] R.K. Cheng, D. Littlejohn, W.A. Nazeer, K.O. Smith, *J. Eng. Gas. Turbines. Power.* 130 (2008) 021501.
[26] R.K. Cheng, D.T. Yegian, M.M. Miyasato, et al., *Proc. Combust. Inst.* 28 (2000) 1305–1313.
[27] A. Marshall, P. Venkateswaran, J. Seitzman, T. Lieuwen, in: 8th U.S. National Combustion Meeting, Park City, Utah, 2013, pp. 15.
[28] R.J. Kee, J.F. Grcar, M. Smooke, J. Miller, *Sandia National Laboratories*, California, Livermore, 1983, pp. 87.
[29] S.G. Davis, A.V. Joshi, H. Wang, F. Egolfopoulos, *Proc. Combust. Inst.* 30 (2005) 1283–1292.
[30] R.J. Kee, J.A. Miller, G.H. Evans, G. Dixon-Lewis, *Proc. Combust. Inst.* 22 (1989) 1479–1494.
[31] A. Amato, M.S. Day, R.K. Cheng, J. Bell, T. Lieuwen, *Central states section spring technical meeting*, Dayton, Ohio, 2012.
[32] S. Pfadler, F. Beyrau, A. Leipertz, *Opt. Expr.* 15 (2007) 15444–15456.
[33] E.R. Hawkes, R. Sankaran, J.H. Chen, *Proc. Combust. Inst.* 33 (2011) 1447–1454.
[34] J. Kerl, C. Lawn, F. Beyrau, *Combust. Flame.* 160 (2013) 2757–2769.
[35] S. Gashi, J. Hult, K.W. Jenkins, et al., *Proc. Combust. Inst.* 30 (2005) 809–817.
[36] N. Otsu, *IEEE Transactions On Systems, Man Cybern.* 9 (1979) 62–66.
[37] T. Poinsot, D. Veynante, *Theoretical and numerical combustion*, RT Edwards Inc, Philadelphia, 2005.
[38] T. Lee, G. North, D. Santavicca, *Combust. Flame.* 93 (1993) 445–456.
[39] C. De Boor, *A Practical guide to splines*, Springer-Verlag, New York, 1978.
[40] P. Craven, G. Wahba, *Numerische math.* 31 (1978) 377–403.
[41] T. Lee, G. North, D. Santavicca, *Combust. Sci. Technol.* 84 (1992) 121–132.
[42] I. Shepherd, W. Ashurst, in, Elsevier, 1992, pp. 485–491.
[43] L. Kostiuk, I. Shepherd, K. Bray, *Combust. Flame.* 118 (1999) 129–139.
[44] M. Haq, C. Sheppard, R. Woolley, D. Greenhalgh, R. Lockett, *Combust. Flame.* 131 (2002) 1–15.
[45] F.T. Yuen, Ö.L. Gülder, *AIAA J.* 47 (2009) 2964–2973.
[46] A. Bonaldo, J.B. Kelman, *Combust. Flame.* 156 (2009) 750–762.
[47] I.G. Shepherd, R.K. Cheng, T. Plessing, C. Kortschik, N. Peters, *Proc. Combust. Inst.* 29 (2002) 1833–1840.
[48] K.W. Jenkins, R.S. Cant, *Proc. Combust. Inst.* 29 (2002) 2023–2029.